

# Probing Causation Dynamics in Quantum Chains near Criticality

Roopayan Ghosh,<sup>1,\*</sup> Bin Yi,<sup>1,2</sup> and  
Sougato Bose<sup>1</sup>

<sup>1</sup>*Department of Physics and Astronomy, University College London, Gower Street, WC1E 6BT London, United Kingdom.*

<sup>2</sup>*Institute of Fundamental and Frontier Sciences, University of Electronic Science and Technology of China, Chengdu 610051, China*  
(Dated: March 29, 2024)

Distinguishing causation from correlation is crucial and requires careful consideration. In this study, we utilize a recent quantum extension of Liang information to investigate causation in quantum chains across their phase diagram. Our analysis encompasses two distinct scenarios: (i) the Aubry-André-Harper model, characterized by a spectrum-wide phase transition, and (ii) the Anisotropic Transverse Field Ising (ANNNI) model, which demonstrates a ground state transition. We discern a notable shift in causation behavior across the critical point with each case exhibiting distinct hallmarks, different from correlation measures. Especially, in the latter case, we observe maximum causation in the ordered phase just preceding the critical point.

**Introduction:** The study of dynamics of quantum many-body systems typically involve the time evolution of correlation functions and the spreading of entanglement [1]. Quantifying causation dynamics in the quantum realm, unlike classical theories, has been challenging [2]. Descriptions of causation dynamics have been mostly limited to quantifying scrambling and relating it to chaos by modifying classical concepts such as the Lyapunov exponents. One such attempt yielded the Out-of-time-ordered-Correlator (OTOC), a reasonably good quantifier of scrambling but having limited applications to identify quantum chaos unlike originally anticipated [3–8]. Hence very recently other modes of quantification of quantum chaos has been proposed [9, 10]. Nevertheless, the adage "correlation does not always imply causation" holds true, and in the context of quantum mechanics, a distinct quantifier for quantum causation remains less established.

Model Hamiltonians of quantum chains provide the microcosm of quantum effects prevalent in our universe. Hence, it is of paramount importance to find a simple detector of causation in these systems, which is easily measurable and can be appropriately connected to the physical intuition born from classical systems. This led to efforts which extract quantum causation from quantum correlations (which are different from the classical correlations), drawing inspiration from the Liang-Kleeman analysis used in classical systems[11]. In classical systems, this analysis was originally formulated with respect to Shannon entropy, and then extended to relative entropy[12], which provides a better measure of predictability than Shannon entropy in certain cases[13–16]. For quantum mechanical systems, this formalism was adapted using von Neumann entropy analogous to Shannon entropy of classical systems.[17] The two big advantages of the quantum version of Liang information over specific observable based correlation measures such as OTOC are (i) the usage of information theoretic tools which makes it more universal, and (ii) it is intuitively

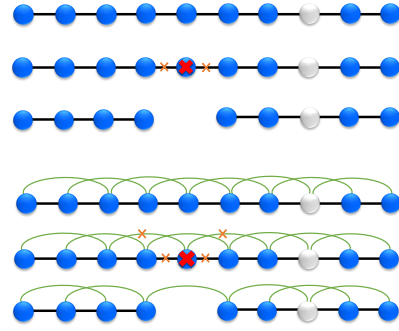


FIG. 1. Schematic diagram of how Liang information flow is computed between two sites by freezing one site (denoted by red cross) and the target site denoted by the white colour. See text for details.

connected to the classical picture, and is practically easy to implement in experimental setups as its simplest version requires single site measurements.

Furthermore, understanding the behaviour of the quantum causation near critical points is completely unexplored. This is the void we wish to fill in this work by using the quantum Liang information formulated with respect to von Neumann entropy as a causation quantifier (note that the direct usage of von Neumann entropy just measures quantum correlations, not causation). To achieve this goal, we conduct simulations of non-trivial dynamics in a quantum state using model Hamiltonians, typically chosen such that their eigenstates exclude the initial state—a scenario known as a quantum quench. While previous research has extensively explored the time evolution of correlation functions for quenches across critical points in quantum many-body systems[18, 19], leveraging non-analyticities in these functions to detect phase transitions[20, 21], to the best of our knowledge, there has been no significant investigation into causality within such a setup. Although some studies involving Out-of-time-ordered-Correlator (OTOC) are available in the

literature[22–24], as mentioned before, their behaviour frequently depends on the choice of operator and we have to be mindful of conservation laws on the system. On the other hand, our study using Liang information suffers from no such drawback and we shall use it to examine the behavior of causation during a quench across critical points in a chain geometry .

**Definitions:** For density operator  $\rho$ , the von Neumann entropy  $S(\rho)$  is defined as:

$$S(\rho) = -\text{Tr}[\rho \log \rho] \quad (1)$$

Consider a bipartite state  $\rho$  evolve under unitary operator  $U(t)$  generated from Hamiltonian function  $H$ , the reduced density state of system AB and subsystems A, B are then denoted  $\rho_{AB}$ ,  $\rho_A$ ,  $\rho_B$ . Following the methodology of its classical counterpart[12], quantum Liang information flow is then given by

$$T_{B \rightarrow A}^r = \frac{dS(\rho_A)}{dt} - \frac{dS(\rho_{AB})}{dt} \quad (2)$$

the cumulative information flow is then

$$\mathbb{T}_{B \rightarrow A} = \int T_{B \rightarrow A}^r dt = \Delta S(\rho_A) - \Delta S(\rho_{AB}). \quad (3)$$

Here  $\rho_{A\bar{B}}$  refers to the density state of A evolving with B frozen[17].

**Setup:** The schematic setup for investigating Liang information flow is illustrated in Fig. 1. We begin by considering a chain with only nearest-neighbor couplings. While the target site can be either a single site or a group, for simplicity, we focus on a single site denoted by the violet marker in the schematic figure throughout this study. In the top three chains, we depict situations with only nearest-neighbor couplings. Removing a site results in a break in the chain, and the effective evolution then occurs within a smaller chain. With longer-range couplings, freezing one site does not break the chain, positioning the target site consistently within the bulk as shown in the bottom three chains.[25].

**Localization transition in Aubry-Andre-Harper model** Liang information, as a measure of causality, proves to be a highly effective tool for delineating the cone of influence in quantum systems. To illustrate, we examine a 1D XX model with a spatially varying on-site magnetic field. The corresponding Hamiltonian is expressed as follows:

$$H = \sum_{j=1}^{L-1} (\sigma_j^x \sigma_{j+1}^x + \sigma_j^y \sigma_{j+1}^y) + \sum_{j=1}^L \mathcal{B}_j \sigma_j^z. \quad (4)$$

where,  $\mathcal{B}_j = \lambda \cos(2\pi\beta j)$ , and  $\beta$  is typically chosen as the inverse golden ratio,  $\beta = \frac{\sqrt{5}-1}{2}$ . The system size  $L$  is typically chosen as a Fibonacci number to minimize finite size effects. This model undergoes a localization-delocalization transition at  $\lambda = 2$  across its eigenspectrum [26].

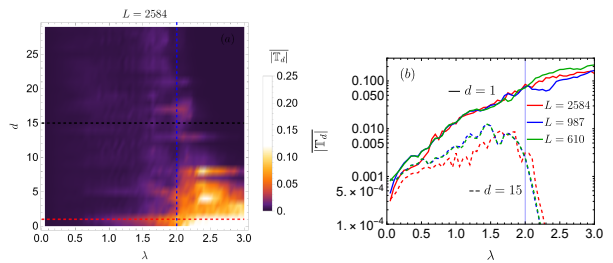


FIG. 2. Cumulative Liang info growth for the model in Eq. (4). (a) We show late time cumulative Liang information to a site  $d$  sites away from the frozen site.  $\overline{\mathbb{T}}_d$  denotes averaged  $\mathbb{T}_d$  for  $t \sim 10^2$ . Averaging is performed to smoothen the plot. The blue dashed line denotes the parameter  $\lambda = 2$  where localization phase transition occurs. (b) The cross section of (a) marked by the red dashed line alongside similar data for other system sizes denoted by different colours. The blue line denotes the critical point. The position of the frozen site is the closest smaller Fibonacci number +1 to  $L$ , i.e. for  $L = 2584$  it is  $i = 1598$  etc.

In Fig. 2, we explore the causal influence of a selected site on other sites across the transition, quantified by cumulative Liang information  $\mathbb{T}_d$  flow over time between two sites separated by a distance  $d$ . The plot is smoothed through an average over  $\mathbb{T}_d$  at timescales beyond the initial transient growth ( $t \sim 10^2$ ). While the frozen site can be arbitrarily chosen for an infinite system, for finite systems as the one utilized in this work, we select the truncated lattice length as the next lowest Fibonacci number to avoid spurious finite size effects from the incommensurate potential. [27]

In Fig. 2(a), we observe that in the delocalized regime, there is equitable Liang information flow from the frozen site to other sites. This corroborates the unrestricted transport expected in this regime as a result of spatially extensive single-particle eigenfunctions. However, as  $\lambda$  approaches the critical point, we note a significant increase in causation effects for nearby sites compared to those farther away. This behavior stems from the restriction of information propagation beyond a certain distance, the localization length. Consequently, local effects strongly influence the evolution of a site. Given that this phase transition occurs across the eigenspectrum, the energy of the chosen initial state minimally affects our findings. Hence, our choice of the Neel state as the initial state for this analysis yields qualitative results similar to those obtained with other typical initial states (see Appendix A).

In Fig. 2(b), we focus on two specific scenarios: (i)  $d = 1$ , representing a nearby site to the frozen site, and (ii)  $d = 15$ , representing a site at a significantly greater distance beyond the localization length of the system. For the site at  $d = 1$ , we observe the anticipated behavior described in the preceding paragraph as  $\lambda$  increases. However for distant sites the causation flow becomes in-

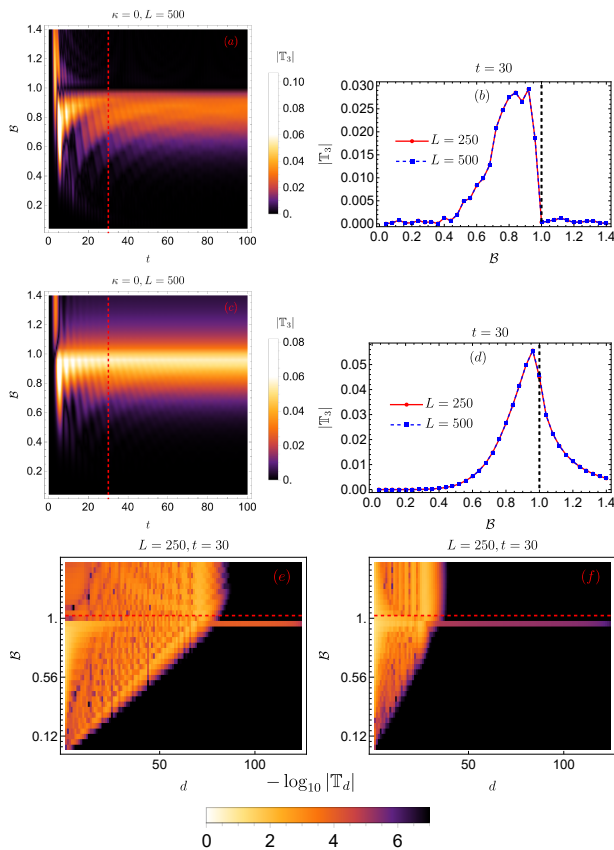


FIG. 3. Variation of absolute value of Liang information for quench to different  $\mathcal{B}$  fields for  $\kappa = 0$ . For (a) and (b) The initial state is chosen to be ground state of  $\mathcal{B} = 0.01$  while for (c) and (d) the initial state is taken to be the ground state of the  $\mathcal{B}$  field at which the Liang information is computed. Fig. (a) shows the value of Liang information  $|\mathbb{T}_3|$ , 3 sites away from the frozen site. The red dashed lines indicate the cross section plotted in Fig. (b), in which the black line indicates the critical point. In (c) and (d) even though we start from an eigenstate, the non-trivial evolution occurs due to the removal of the frozen site, and is used to compute the causation flow. (e) and (f) shows the spatial profile of Liang information for quenches for  $L = 250$  at a chosen time instance. (e) has same setup as (a),(b) and (f) has the same setup as (c),(d). The red dashed line indicates the critical point  $\mathcal{B}_c = 1$

interesting near criticality. For small  $\lambda$ , the behavior mirrors that of nearby sites i.e. there is a gradual increase in cumulative Liang information with  $\lambda$  until approximately  $\lambda \sim 1.5$ . This is followed by a plateau before the expected sharp decline in the localized regime. The intriguing aspect is the occurrence of a peak in causality for  $\lambda < 2$  for distant sites, which seems to slowly drift towards  $\lambda \sim 1.5$  for larger values of  $d$  as seen in Fig. 2(a), from the faint violet regions. The larger causation values indicate an already inequitable flow of information between different sites in the said parameter regime. This in turn signifies traces of localization in the parts of the system acting as a herald to the onset of localization across the spectrum

for  $\lambda = 2$ . However, it is not fully clear whether this effect holds in the thermodynamic limit, even though a naive finite size analysis in Fig. 2(b) suggests it is not dependent on size. Furthermore, for  $\lambda > 2$  exponentially localized wavefunctions result in exponentially small information leakage with  $d$  beyond the localization length, whose signature is given by a rapid but continuous decrease in Liang information with  $d$ .

#### Ground state phase transitions in Ising models:

The localization phase transition in the previous example demonstrated the goodness of Liang information to measure causation, which encourages us to study it in more complicated settings. So we next direct our focus to the Anisotropic Next Nearest Neighbor Ising (ANNNI) model. This model includes a next-nearest-neighbor coupling, is non-integrable, and lacks  $U(1)$  symmetry present in the previous example. In certain parameter regimes, the ground state of this model undergoes a ferromagnetic to paramagnetic Ising phase transition upon tuning the transverse magnetization strength. In the following analysis, we will investigate the influence of the middle site of the chain on other chosen sites across different parameter regimes. Generalizing this study to encompass the influence over multiple sites is straightforward.

The Hamiltonian of ANNNI chain is given by,

$$H_L = - \sum_j^{L-1} \sigma_j^z \sigma_{j+1}^z + \kappa \sum_j^{L-2} \sigma_j^z \sigma_{j+2}^z - \mathcal{B} \sum_j^L \sigma_j^x, \quad (5)$$

where  $\kappa$  represents the strength of the next-nearest neighbor term and  $\mathcal{B}$  is the magnitude of magnetic field applied along the transverse axis and  $L$  denotes the number of sites in the system.

At fixed value of  $0 < \kappa < 0.5$ , the ground state of the ANNNI model undergoes quantum phase transition from the ferromagnetic phase to the paramagnetic phase when transverse field  $\mathcal{B} > 0$  exceeds a critical value  $\mathcal{B}_c$ . The phase transition point has been computed before[28–33] and the critical parameters  $\kappa_c$  and  $\mathcal{B}_c$  are known to satisfy:

$$1 - 2\kappa_c = \mathcal{B}_c - \mathcal{B}_c^2 \frac{\kappa_c}{2 - 2\kappa_c} \quad (6)$$

While the quantum phase transition is traditionally considered an equilibrium phenomenon occurring in the ground state, previous studies [20, 21, 34, 35] have demonstrated that signatures of this transition can manifest in non-equilibrium quantum quenches. In the present work, motivated by the understanding of heightened quantum sensitivity near phase transitions[36], we actively seek these signatures within the causation measure Liang information.

Since the model in Eq. (5) is non-integrable for generic parameter values we will resort to numerical simulations (exact diagonalization, TDVP and DMRG) for our results. However at the special point  $\kappa = 0$ , it reduces

to the integrable transverse Ising model. We first visit the growth of Liang information in this integrable chain before discussing the results for  $\kappa > 0$ .

$\kappa = 0$  case: For  $\kappa = 0$ , we can use a canonical transformation ( $\sigma^x \rightarrow \sigma^z, \sigma^z \rightarrow -\sigma^x$ ) and then a Jordan-Wigner transformation to map the  $H_L$  to a system of spinless fermions,

$$H_L = -\frac{1}{2} \sum_{i=1}^{L-1} [c_i^\dagger c_{i+1} + c_i^\dagger c_{i+1}^\dagger + \text{h.c.}] - \mathcal{B} \sum_{i=1}^L (c_i^\dagger c_i - \frac{1}{2}) \quad (7)$$

where  $c_i [c_i^\dagger]$  is the spinless JW fermion annihilation [creation] operator. Since we are interested in the influence on a single site, we require the one site density matrix which in this special case is given by[37],

$$\rho_j = \frac{\mathbb{I} + \langle \sigma_j^z \rangle \sigma^z}{2}, \quad (8)$$

where  $\langle \sigma_j^z \rangle = 2\langle c_j^\dagger c_j \rangle - 1$ . Furthermore since the Hamiltonian is quadratic in fermionic operators, the time evolution of this quantity can be found semi-analytically. Details of the computation are provided in Appendix B

The results for such a system starting from different initial states are shown in Fig. 3. In Fig. 3(a) we show the growth of Lianginfo three sites away from the frozen site (chosen to be the middle site of the full lattice) when the initial state is chosen to be the ground state at  $\mathcal{B} = 0.01$  and we quench to different values of  $\mathcal{B}$ . When  $\mathcal{B}$  is small, we are far away from criticality. The initial state in this regime has large overlap with the ground state, and the causal influence of one site over another during evolution is very limited as evolution itself is limited. This gradually changes as we increase  $\mathcal{B}$  towards  $\mathcal{B}_c$  as we expect maximum sensitivity near the critical point. On the other extreme for very large  $\mathcal{B}$  the system has only local evolution, so we expect Liang information to again be small during time evolution. This is the qualitative behaviour we notice in Fig. 3(b). While the peak of causation is distinct it appears to be quite shifted from the critical  $\mathcal{B}_c = 1$ . Naively we might identify the reason for this anomaly to be our choice of initial state, which has finite overlaps several high energy states that do not possess the desired features at criticality. To prevent this one can choose the initial state to always be the ground state of the corresponding  $\mathcal{B}$ , the results of which is shown in Figs. 3 (c) and (d). However the peak still occurs for  $\mathcal{B}_p < \mathcal{B}_c$ , even though now  $\mathcal{B}_p$  shifts to larger values.

The strongest indicator is shown in Fig. 3(e) and (f) where we study how the frozen site influences sites at different distances. Clearly for quenches at  $\mathcal{B}_p$ , the chosen site influences other sites at all lengthscales. This is a hallmark of criticality for second order phase transitions, the divergence of correlation length, which in turn means correlations and thus entanglement develop at all length scales. While typically such a behaviour is seen in equilibrium properties of the ground state, this phenomenon

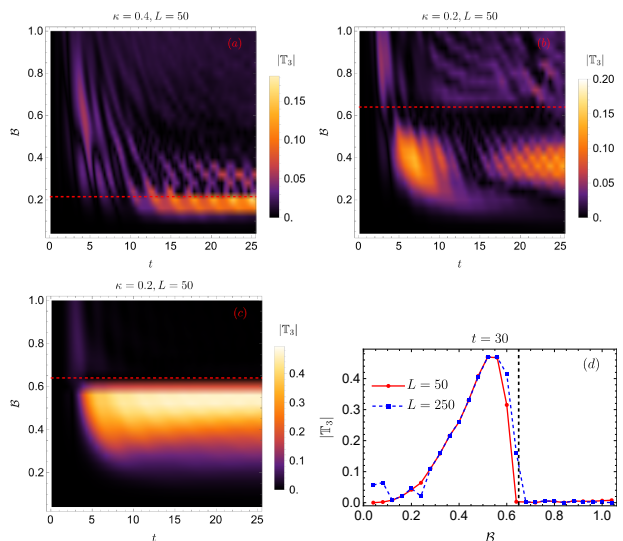


FIG. 4. Variation of absolute value of Liang information for quench to different  $\mathcal{B}$  field with constant  $\kappa \neq 0$  for system size of  $L = 50, 250$  computed via TDVP<sup>a</sup>. (a) Liang information  $|T_3|$ , 3 sites away from the frozen site when the initial state is chosen to be ferromagnetic state  $|\downarrow\downarrow \dots \downarrow\rangle$ , and  $\kappa = 0.4$ . (b)  $|T_3|$  for  $\kappa = 0.2$  starting from the same initial state. (c)  $|T_3|$  for  $\kappa = 0.2$  starting from the ground state, similar to Fig. 3(c). (d) Cross section of (c) at  $t = 30$  compared with  $|T_3|$  for a larger system size,  $L = 250$ . The red/black dashed lines represent  $\mathcal{B}_c$  computed from Eq. (6).

<sup>a</sup> parameters- cutoff=  $10^{-7}$ ,  $dt = 0.01$ ,  $\chi$  or bond dimension was capped at 5000.

still shows up in Liang information, a non-equilibrium quantity, remarkably well irrespective of the initial state.

$\kappa > 0$  case: For  $\kappa > 0$  one can perform quenches in  $\mathcal{B}$  keeping  $\kappa$  constant or vice-versa. Both yield qualitatively similar results (see also Appendix D). In Fig. 4 we demonstrate that features shown by Liang information in the non-interacting case continue to persist for the non-integrable interacting model. As in the previous section we study two scenarios: the ferromagnetic initial state  $|\downarrow\downarrow\downarrow \dots \downarrow\rangle$  which is the ground state at  $\kappa = \mathcal{B} = 0$ , and the local quench from the ground state of corresponding  $\mathcal{B}$ . We also add a very small longitudinal field to prevent any degeneracy for small values of  $\mathcal{B}$ .

In Fig. 4(a) we notice that inspite of starting from the ferromagnetic initial state for much smaller  $L = 50$  compared to Fig. 3, Liang information shows a peak just before criticality. (in fact for  $\kappa = 0$ , this small system size shows noisy data). The reason for the closeness of the peak to the critical point compared to the  $\kappa = 0$  case is that, larger  $\kappa$  pushes the critical point towards  $\mathcal{B} = 0$ . Then even at these system sizes this initial state maintains sufficient overlap with the ground state of the Hamiltonian before the critical point to exhibit the expected behaviour.

But as we decrease  $\kappa$  to 0.2, there remains no corre-

lation between the maxima and the critical point, which is denoted by the red dashed lines. This is expected as the critical point moves to larger  $\mathcal{B}$ , the initial state no longer remains a low energy state and thus cannot respond to phase transition in ground states. Furthermore since this model is non-integrable, lack of conservation laws allows exploration of more of Hilbert space compared to the  $\kappa = 0$  model leading to greater deviations than that case.

However, we do recover the peak just before criticality phenomena once we start from the ground state, shown in Figs. 4(c),(d), just as we did for  $\kappa = 0$ , for even smaller system sizes. (See Appendix D for other parameters). It is clear that for all  $\kappa$  which supports phase transition, the maxima typically occurs at  $\mathcal{B}_p \neq \mathcal{B}_c$  ( $\mathcal{B} < \mathcal{B}_c$  for all the cases considered here), distinguishing causation from correlation. While correlation length of the ground state can indeed diverge at the critical point, the causation dynamics can maximize at slightly different values, as it is governed by the competing behaviour of the various Hamiltonian terms on the initial state. Of course the correlation lengthscales still plays a crucial part in causation dynamics, more so in the integrable model and for the ground state initial state where such non-analyticities are stronger, shown by the closeness in  $\mathcal{B}_p$  and  $\mathcal{B}_c$  in these cases. Further analytical insights may be obtained by finding a mean field mapping of  $\kappa \neq 0$  model to the solvable transverse Ising model[34], but it is left as a future endeavour.

**Discussion:** In this work we have studied causation behaviour of different sites in quantum chains by studying the cumulative Liang information flow between them. Specifically, we study the parameter regime where we find a peak in cumulative Liang information indicating a causality peak. The causality peaks do not necessarily correspond to a maxima in correlation of the corresponding sites, but rather roughly detects the maxima in difference of expectation values of local operators with and without the site whose influence we want to compute. We have showed that this measure successfully showcases the democracy of influence in the fully delocalized regime and near-site causation in localized regime in one dimensional Aubry Andre Harper model. Furthermore it even responds to the diverging correlation lengths in ground state second order phase transitions of the next-nearest neighbour Ising model. Our most crucial find is that the peak of causation does not occur exactly at the critical point, but rather slightly towards the ordered side of the transition, for quenches from the ordered side. Thus causation flow encapsulated by quantum Liang information between two sites is a new non-equilibrium herald of an equilibrium phase transition.

While classical Liang information analysis is a well-established approach to quantify causation in classical networks, its applicability in quantum systems is an area that is just beginning to be explored. This work rep-

resents an initial exploration, focusing on two specific quantum systems. One can immediately see that Liang information analysis can provide a natural test bed for the analysis of many-body localization transitions, for instance, it can be employed to identify resonances between sets of sites that induce the avalanche breakdown of localization in different geometries. There are also open questions regarding its behaviour in the vicinity of topological phase transitions, and in higher dimensional quantum systems including complex networks.

RG thanks Krishnendu Sengupta, Arnab Das and Madhumita Sarkar for discussions. RG and SB acknowledge the EPSRC grants Nonergodic quantum manipulation EP/R029075/1 and Many-Body Phases In Continuous-Time Quantum Computation EP/Y004590/1 for support .

---

\* ucaprgh@ucl.ac.uk

- [1] A. Polkovnikov, K. Sengupta, A. Silva, and M. Vengalattore, Colloquium: Nonequilibrium dynamics of closed interacting quantum systems, *Rev. Mod. Phys.* **83**, 863 (2011).
- [2] Č. Brukner, Quantum causality, *Nature Physics* **10**, 259 (2014).
- [3] J. Maldacena, S. H. Shenker, and D. Stanford, A bound on chaos, *Journal of High Energy Physics* **2016**, 106 (2016).
- [4] I. Kukuljan, S. Grozdanov, and P. Tomaž, Weak quantum chaos, *Phys. Rev. B* **96**, 060301 (2017).
- [5] A. W. Harrow, L. Kong, Z.-W. Liu, S. Mehraban, and P. W. Shor, Separation of out-of-time-ordered correlation and entanglement, *PRX Quantum* **2**, 020339 (2021).
- [6] J. Riddell and E. S. Sørensen, Out-of-time ordered correlators and entanglement growth in the random-field xx spin chain, *Phys. Rev. B* **99**, 054205 (2019).
- [7] T. Notenson, I. Garcia-Mata, A. J. Roncaglia, and D. A. Wisniacki, Classical approach to equilibrium of out-of-time ordered correlators in mixed systems, *Phys. Rev. E* **107**, 064207 (2023).
- [8] T. Xu, T. Scaffidi, and X. Cao, Does scrambling equal chaos?, *Phys. Rev. Lett.* **124**, 140602 (2020).
- [9] M. Pandey, P. W. Claeys, D. K. Campbell, A. Polkovnikov, and D. Sels, Adiabatic eigenstate deformations as a sensitive probe for quantum chaos, *Phys. Rev. X* **10**, 041017 (2020).
- [10] C. Lim, K. Matirko, A. Polkovnikov, and M. O. Flynn, Defining classical and quantum chaos through adiabatic transformations (2024), [arXiv:2401.01927 \[cond-mat.stat-mech\]](https://arxiv.org/abs/2401.01927).
- [11] X. San Liang, Information flow and causality as rigorous notions ab initio, *Physical Review E* **94**, 052201 (2016).
- [12] X. S. Liang, Causation and information flow with respect to relative entropy, *Chaos: An Interdisciplinary Journal of Nonlinear Science* **28**, 075311 (2018).
- [13] T. Schneider and S. M. Griffies, A conceptual framework for predictability studies, *Journal of climate* **12**, 3133 (1999).
- [14] R. Kleeman, Measuring dynamical prediction utility us-

- ing relative entropy, *Journal of the atmospheric sciences* **59**, 2057 (2002).
- [15] R. Kleeman and A. Majda, Predictability in a model of geophysical turbulence, *Journal of the atmospheric sciences* **62**, 2864 (2005).
- [16] R. Kleeman, Limits, variability, and general behavior of statistical predictability of the midlatitude atmosphere, *Journal of the atmospheric sciences* **65**, 263 (2008).
- [17] B. Yi and S. Bose, Quantum Liang information flow as causation quantifier, *Physical Review Letters* **129**, 020501 (2022).
- [18] K. Sengupta, S. Powell, and S. Sachdev, Quench dynamics across quantum critical points, *Phys. Rev. A* **69**, 053616 (2004).
- [19] P. Basu and S. R. Das, Quantum quench across a holographic critical point, *Journal of High Energy Physics* **2012**, 103 (2012).
- [20] A. Haldar, K. Mallayya, M. Heyl, F. Pollmann, M. Rigol, and A. Das, Signatures of quantum phase transitions after quenches in quantum chaotic one-dimensional systems, *Phys. Rev. X* **11**, 031062 (2021).
- [21] C. B. Dağ, P. Uhrich, Y. Wang, I. P. McCulloch, and J. C. Halimeh, Detecting quantum phase transitions in the quasistationary regime of Ising chains, *Phys. Rev. B* **107**, 094432 (2023).
- [22] H. Shen, P. Zhang, R. Fan, and H. Zhai, Out-of-time-order correlation at a quantum phase transition, *Phys. Rev. B* **96**, 054503 (2017).
- [23] Z.-H. Sun, J.-Q. Cai, Q.-C. Tang, Y. Hu, and H. Fan, Out-of-Time-Order Correlators and Quantum Phase Transitions in the Rabi and Dicke Models, *Annalen Phys.* **532**, 1900270 (2020).
- [24] M. Heyl, F. Pollmann, and B. Dóra, Detecting equilibrium and dynamical quantum phase transitions in Ising chains via out-of-time-ordered correlators, *Phys. Rev. Lett.* **121**, 016801 (2018).
- [25] To prevent chain breakage upon freezing site  $p$ , one must ensure couplings of range  $p + 1$  in a chain with open boundary conditions. For periodic boundary conditions, there is a connection between sites 1 and  $L$ , preventing chain breakage but transforming the system into an open boundary condition system upon freezing a site. However, we opt for open boundary conditions in this work to avoid this additional complexity. Although it should not significantly differ from the results in this work for unitary evolution, discrepancies may arise in the non-unitary scenario, particularly where potential skin effects emerge. We plan to explore these differences in a subsequent study.
- [26] S. Aubry and G. André, Analyticity breaking and Anderson localization in incommensurate lattices, (1980).
- [27] To avoid cutting the chain one can consider a power law decaying hopping model instead with large power  $\sim O(10)$ , such that the phase transition point remains near  $\lambda = 2$ . We have verified (not shown) that this does not affect the results qualitatively.
- [28] W. Selke, The Annni model — theoretical analysis and experimental application, *Physics Reports* **170**, 213 (1988).
- [29] S. Suzuki, J.-i. Inoue, and B. K. Chakrabarti, Annni model in transverse field, in *Quantum Ising Phases and Transitions in Transverse Ising Models* (Springer Berlin Heidelberg, Berlin, Heidelberg, 2013) pp. 73–103.
- [30] D. Allen, P. Azaria, and P. Lecheminant, A two-leg quantum Ising ladder: a bosonization study of the Annni model, *Journal of Physics A: Mathematical and General* **34**, L305 (2001).
- [31] A. Nagy, Exploring phase transitions by finite-entanglement scaling of MPS in the 1d Annni model, *New Journal of Physics* **13**, 023015 (2011).
- [32] P. R. C. Guimarães, J. a. A. Plascak, F. C. Sá Barreto, and J. a. Florencio, Quantum phase transitions in the one-dimensional transverse Ising model with second-neighbor interactions, *Phys. Rev. B* **66**, 064413 (2002).
- [33] M. Beccaria, M. Campostrini, and A. Feo, Density-matrix renormalization-group study of the disorder line in the quantum axial next-nearest-neighbor Ising model, *Phys. Rev. B* **73**, 052402 (2006).
- [34] J. H. Robertson, R. Senese, and F. H. L. Essler, A simple theory for quantum quenches in the ANNNI model, *SciPost Phys.* **15**, 032 (2023).
- [35] C. B. Dağ, Y. Wang, P. Uhrich, X. Na, and J. C. Halimeh, Critical slowing down in sudden quench dynamics, *Phys. Rev. B* **107**, L121113 (2023).
- [36] P. Zanardi and N. Paunković, Ground state overlap and quantum phase transitions, *Phys. Rev. E* **74**, 031123 (2006).
- [37] T. J. Osborne and M. A. Nielsen, Entanglement in a simple quantum phase transition, *Phys. Rev. A* **66**, 032110 (2002).
- [38] R. Ghosh and A. Das, Disorder-induced enhancement of entanglement growth in one dimension: Information leakage at the scale of the localization length, *Phys. Rev. B* **103**, 024202 (2021).
- [39] I. Peschel, Calculation of reduced density matrices from correlation functions, *Journal of Physics A: Mathematical and General* **36**, L205 (2003).
- [40] I. Peschel and V. Eisler, Reduced density matrices and entanglement entropy in free lattice models, *Journal of Physics A: Mathematical and Theoretical* **42**, 504003 (2009).
- [41] E. Lieb, T. Schultz, and D. Mattis, Two soluble models of an antiferromagnetic chain, *Annals of Physics* **16**, 407 (1961).
- [42] M. Kormos, Inhomogeneous quenches in the transverse field Ising chain: scaling and front dynamics, *SciPost Phys.* **3**, 020 (2017).
- [43] One can also rewrite them in terms of Majorana fermions and perform the same computation.

### Appendix A: Initial state independence of Aubry-Andre model results

In Fig. 5 we choose two random computational initial states for system size  $L = 987$  at approximately half filling  $\sum_i \sigma_i^z = 1$  and show the behaviour of smoothed time averaged Liang information  $\overline{\mathbb{T}}_d$  with distance  $d$  from the frozen site. Evidently, the qualitative nature of all the cases are the same, but there are a few quantitative differences in causation flow based on the initial state, which is picked up by Liang information. Specifically near the localization transition  $\lambda \sim 1.5 - 2$ , the loss of democracy in causality for different initial states differs slightly from each other. Indeed, all initial states cannot be expected to relax exactly equivalently, for example,

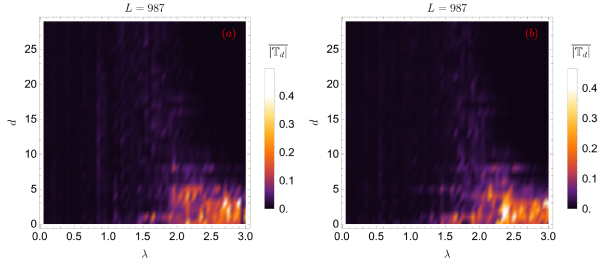


FIG. 5. Demonstration of cumulative Liang information flow for Aubry Andre model, similar to Fig. 2

atypical states such as the domain wall states have very different information leakage during evolution compared to Neel states.[38] This shows up as small quantitative differences in flow of Liang information for states at intermediate distance from the frozen site as seen in the figure.

### Appendix B: Details of computation for open Ising chain

The nearest neighbour transverse Ising model Hamiltonian,

$$H = - \sum_j^{L-1} \sigma_j^z \sigma_{j+1}^z - \mathcal{B} \sum_j^L \sigma_j^x, \quad (\text{B1})$$

after the JW transformation is a Hamiltonian quadratic in fermionic operators.

$$H = -\frac{1}{2} \sum_{i=1}^{L-1} [c_i^\dagger c_{i+1} + c_i^\dagger c_{i+1}^\dagger + \text{h.c.}] - \mathcal{B} \sum_{i=1}^L (c_i^\dagger c_i - \frac{1}{2}) \quad (\text{B2})$$

Hence the entanglement entropy of a subsystem can be computed just from the two point correlation functions[39, 40]  $\langle c_i^\dagger c_j \rangle$  and  $\langle c_i^\dagger c_j^\dagger \rangle$ . In our case this further simplifies to just computing  $\langle c_j^\dagger c_j \rangle$  since we are just interested in computing influence on one site i.e. the subsystem consists of just one site. In fact it can be shown that[37] the one site density matrix in such a system is given by,

$$\rho_j = \frac{\mathbb{I} + \langle \sigma_j^z \rangle \sigma^z}{2}, \quad (\text{B3})$$

where  $\langle \sigma_j^z \rangle = 2 \langle c_j^\dagger c_j \rangle - 1$ . Since we are using open boundary conditions, momentum  $k$  is no longer a good quantum number, hence this Hamiltonian cannot be block diagonalized by the Fourier transformation. However using the quadratic nature of the Hamiltonian we can construct the eigenmodes of the system analytically as follows[41, 42].

We define two new fermionic operators[43] for convenience,

$$A_i = (c_i^\dagger + c_i), \quad B_i = (c_i^\dagger - c_i), \quad (\text{B4})$$

the Eq. (5) becomes,

$$H = \frac{1}{2} \sum_i^{L-1} A_{i+1} B + \frac{h}{2} \sum_i A_i B_i \quad (\text{B5})$$

and we can compute the two point correlations functions such as  $\langle \sigma_j^z \rangle = -\langle A_j B_j \rangle$  appropriately.

Then  $H$  in Eq. B2 can be immediately diagonalized to

$$H_D = \sum_j \epsilon_k \eta_k^\dagger \eta_k + \text{const.} \quad (\text{B6})$$

where  $\epsilon_k = \sqrt{1 - 2\mathcal{B} \cos k + \mathcal{B}^2}$ , by the real linear transformation,

$$\eta_k = \frac{1}{2} \sum_j [\phi_{kj} A_j - \psi_{kj} B_j] \quad (\text{B7})$$

with

$$\begin{aligned} \phi_{kj} &= -\mathcal{N}_k (-1)^n \sin[k(L+1-j)] \\ \psi_{kj} &= -\mathcal{N}_k \sin[kj]. \end{aligned} \quad (\text{B8})$$

Here the  $k \in [0, \pi]$  modes are obtained from the  $n^{\text{th}}$  (This is the same  $n$  as in Eq. (B8)) solution of the equation,

$$\frac{\sin[(L+1)k]}{\sin[Lk]} = -\frac{1}{\mathcal{B}} \quad (\text{B9})$$

and  $\mathcal{N}_k$  is the normalization constant given by,

$$\mathcal{N}_k = \frac{1}{\sqrt{\frac{L}{2} + \frac{\mathcal{B}(\mathcal{B} + \cos k)}{2\epsilon_k^2}}}.$$

Note that for  $\mathcal{B} \rightarrow \infty$ ,  $k \sim \frac{\pi n}{L+1}$ ,  $n = 1, \dots, L$ . Note that for  $\mathcal{B} > 1$  Eq. (B9) always supports real valued solutions, but it can have an imaginary solution for  $\mathcal{B} < 1$ . Clearly the imaginary value of  $k$  indicates the wavefunction is localized, and it happens at the edges. For further details on construction of this localized solution refer 42. This aspect is not relevant for our computations. Now we shall compute the time evolution of  $\langle c_i^\dagger c_i \rangle$  to understand the time evolution of the reduced density matrix. This can be done in the following steps.

1.  $\langle A_j(t) B_j(t) \rangle = \langle (c_j^\dagger)^2 + 1 - 2c_j^\dagger(t) c_j(t) - (c_j)^2 \rangle = -\langle \sigma_j^z(t) \rangle$  where we have used that  $c_j [c_j^\dagger]$  are fermionic annihilation [creation] operators.
2.  $\langle A_j(t) B_j(t) \rangle$  can be written in terms of the Bogoliubov quasiparticles,

$$\langle A_j(t) B_j(t) \rangle = \sum_{k,l=1}^L \phi_{kj} \psi_{lj} \langle (\eta_k^\dagger(t) + \eta_k(t)) (\eta_l(t)^\dagger - \eta_l(t)) \rangle$$

3. Now  $\eta(t)$  and  $\eta^\dagger$  being the quasiparticles of the Hamiltonian has a very simple time evolution,

$$\eta_k^\dagger(t) = e^{i\epsilon_k t} \eta_k^\dagger(0)$$

which can be substituted in the previous expression.

4. The next step is to rotate the expression back to the  $A, B$  basis to obtain

$$\begin{aligned} \langle A_j(t)B_j(t) \rangle &= -\frac{1}{2} \sum_{m,n,k,l} \phi_{kj} \psi_{lj} \phi_{kn} \psi_{lm} \langle A_n(0)B_m(0) \rangle (\cos[t(\epsilon_k + \epsilon_l)] + \cos[t(\epsilon_k - \epsilon_l)]) \\ &\quad - \frac{1}{2} \sum_{m,n,k,l} \phi_{kj} \psi_{lj} \psi_{kn} \phi_{lm} \langle B_n(0)A_m(0) \rangle (\cos[t(\epsilon_k + \epsilon_l)] - \cos[t(\epsilon_k - \epsilon_l)]) \end{aligned} \quad (\text{B10})$$

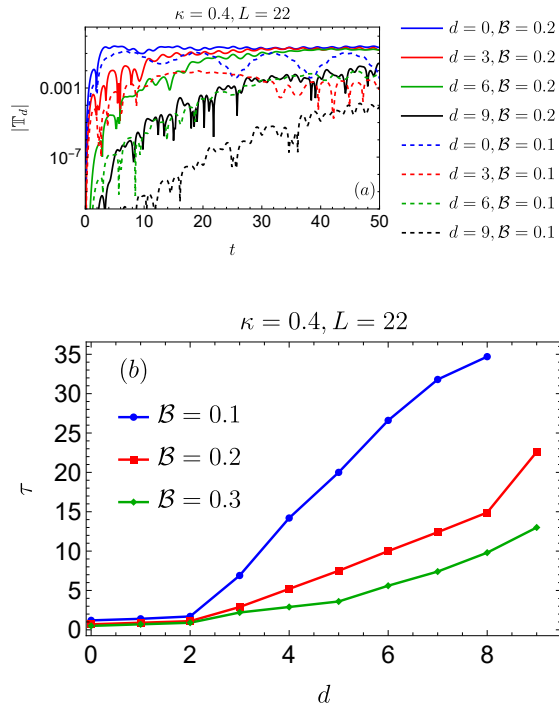


FIG. 6. (a) The variation of the magnitude of Liang information at a distance  $d$  from the frozen site.  $d = 0$  denotes the site next to the frozen site for a quench from the ferromagnetic ground state  $|\downarrow\downarrow \dots \downarrow\rangle$  to  $\mathcal{B} = 0.1$  and  $\kappa = 0.4$ . (b) Plot of  $\tau$ , the time at which  $\mathbb{T}_d \geq 0.001$  for quenches to different values of  $\mathcal{B}$  for  $\kappa = 0.4$ . the system size chosen is  $L = 50$ .

Here while indices  $j, m, n$  can take any integer values in  $[1, L]$ ,  $k, l$  label the eigenmodes obtained by solving Eq. (B9). In our case (see Fig.1), since we remove one site for the system, this amounts to a change in  $L$  and  $j$  to  $L'$  and  $j'$  of the system. This means upon removal of site  $\langle A_j(0)B_m(0) \rangle$  will require the available indices restricted to  $L'$  with  $j$  changing to  $j'$  reflecting the new position of the same site on the truncated chain.

### Appendix C: Lightcones in the ANNNI model

Let us examine the causality light cones obtained for the next-nearest neighbor ANNNI model. For this purpose, we choose representative values of  $\mathcal{B}$  and  $\kappa$  in Fig. 6 for the quench and study the evolution of Liang information across different sites in the chain. The initial state is chosen to be the ferromagnetic state,  $|\downarrow\downarrow \dots \downarrow\rangle$ . As anticipated, on the site closest to the frozen site ( $d = 0$ ), we observe an immediate growth of Liang information, with the growth occurring at later times as we move to sites with increasing distance. This characteristic pattern is a hallmark of local Hamiltonians. Furthermore, there is larger causation flow for  $\mathcal{B} = 0.2$  than for  $\mathcal{B} = 0.1$ , since  $\mathcal{B} = 0.2$  is closer to the critical point  $\mathcal{B}_c = 0.21$ . This is specially apparent for the  $d = 3, 6$  cases where  $|\mathbb{T}_d|$  shows values which differ by several orders of magnitude for the two cases.

In Fig. 6(b) we define  $\tau$  such that  $|\mathbb{T}_d| < 0.001$  for  $t < \tau$  and plot its variation with  $\mathcal{B}$  and distance  $d$ . We observe an interesting behaviour that  $\tau$  for same  $d$  becomes smaller as we increase  $\mathcal{B}$ . We have also verified that the even smaller choices of cutoff does not qualitatively change our results. This result can seem surprising since we have claimed causation peak is observed for quenches to  $\mathcal{B}$  which is just smaller than  $\mathcal{B}_c$ , but we see a decrease in  $\tau(d)$  with  $\mathcal{B}$ , which seems to suggest the influence of sites maximize beyond critical quenches. But upon closer look we realize that this is just a transient effect which is also seen in Fig. 4. Indeed since the initial state is an eigenstate for  $\mathcal{B} = 0$ , in the initial stages of quench to intermediate  $\mathcal{B}$ , the initial undergoes non-trivial evolution which reflects in the significant influence of different sites on the chosen site during evolution. Relaxation typically occurs faster for larger  $\mathcal{B}$ , which in turn indicates smaller observed values of  $\tau$ . But beyond the transient relaxation period the sites exert very little influence, as the system has completely relaxed. And furthermore large  $\mathcal{B}$  makes the Hamiltonian effectively on-site, so each spin effectively evolves independently. On the opposite extreme, for small  $\mathcal{B}$ , where the initial state has a very large overlap with one of the eigenstates of the Hamiltonian for both the ordinary and frozen system. Hence the

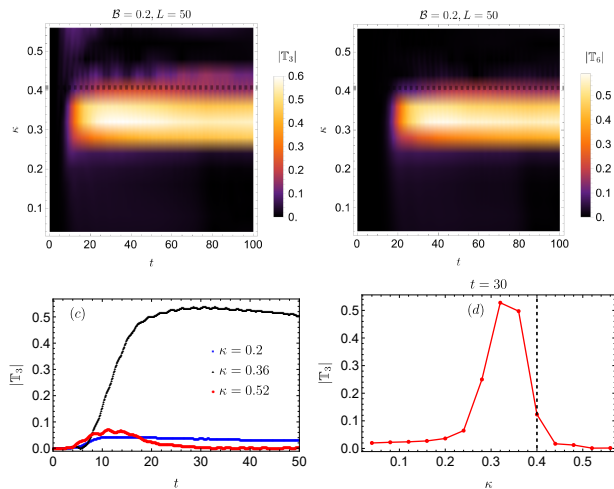


FIG. 7. Variation of absolute value of Liang information for quench to different  $\kappa$  fields with constant  $B = 0.2$ . The initial state is chosen to be ferromagnetic state, i.e. eigenstate of  $\mathcal{B} = \kappa = 0$ . Fig. (a) shows the value of Liang information  $|\mathbb{T}_3|$ , 3 sites away from the frozen site. the black dashed lines indicate the cross sections plotted in Fig.(c), the red dashed line indicates the cross section plotted in Fig.(d). Fig.(b) is same as Fig.(a) except the distance is 6 sites.

evolution is slow, and the slope is larger.

## Appendix D: Results for quenches to other parameters

### 1. Quench in $\kappa$ from ferromagnetic state

In this section, we discuss the effect of the nature of the quench by studying the variation of Liang information flow while quenching to a specific  $\mathcal{B}$  but varying  $\kappa$ . The results are shown in Fig. 7, where we quench to  $\mathcal{B} = 0.2$  with varying  $\kappa$ . From Eq. 6, we expect  $\kappa_c \sim 0.4$ . Hence, using similar arguments as before, we expect Liang information to show a sharp rise close to  $\kappa_c$  before showing a sharp decrease for  $\kappa > \kappa_c$ , a feature evident in Fig. 7(a), (b), and (d). As expected from the previous section, the Liang information of the farther site,  $|\mathbb{T}_6|$  shows slightly lower sensitivity to the critical point than  $|\mathbb{T}_3|$ . Also, one can clearly see the light-cone effect, which causes the Liang info to rise at later times for the more distant site. In Fig. 7(c), we plot the growth for three values of  $\kappa$  and see that remarkably, for values of  $\kappa$  close but less than  $\kappa_c$ , we almost saturate the Liang information growth, indicating that the entanglement growth becomes fully different between the unfrozen site and frozen site scenarios.

This stems from the still large overlap of the initial state with the ground state eigenfunction in the unfrozen case, while a significant change occurs in the frozen case. Comparing to the quench in  $\mathcal{B}$ , changing  $\kappa$  while keeping  $\mathcal{B}$  constant causes the evolution of the site-frozen system

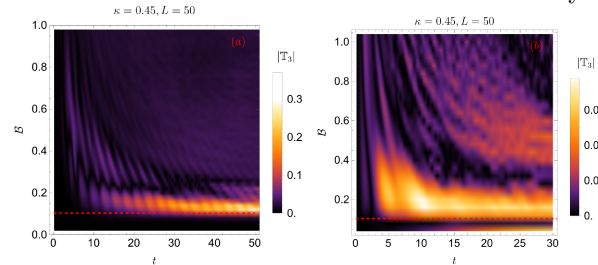


FIG. 8. Variation Liang formation when the quench is for  $\kappa = 0.45$ . (a) The initial state is the ferromagnetic state. All the rest of the parameters are same as Fig. 4(a). (b) The initial state is the ground state of the corresponding  $\mathcal{B}$ , the rest of the parameters are same as Fig. 4(c)

to change more than changing  $\mathcal{B}$  just before the critical point. This is possibly because while  $\mathcal{B}$  is just an on-site term,  $\kappa$  connects two sites and thus shows an enhanced response when Liang information is computed.

### 2. Further results for quenches in $\mathcal{B}$

In Fig. 8 we plot the scenario for quenches in  $\mathcal{B}$  when  $\kappa = 0.45$ . In (a) we show the case when we start from the ferromagnetic state, and since the critical point is for even smaller  $\mathcal{B}$  than when  $\kappa = 0.4$ , such an initial state gives good response near the critical point, comparable to the case when we start from the ground state of corresponding  $\mathcal{B}$  which is shown in (b). Interestingly it seems that here starting from the ground state gives a weaker signal than starting from the ferromagnetic state. This is possibly due to the  $\mathcal{B}_c \sim 0$  making the on site spin flip term of weaker strength. This evolution very slow in this case and we possibly need to go to much larger timescales to have a conclusive result which is beyond the scope of ordinary tensor network algorithms. Finally in Fig. 9 we show more cases of the ‘peak before critical point’ phenomena computing the Liang information flow between sites separated by a distance  $d = 3$  starting from the ground state. These results further corroborate our conclusions in the main text. Additionally note how the growth of Liang information near the point of criticality occurs at an earlier timescale for smaller  $\kappa$ , which showcases how larger  $\mathcal{B}$ , induces spin flip processes at a smaller timescale causing dynamics, if existent, to speed up, creating a light cone with a greater slope.

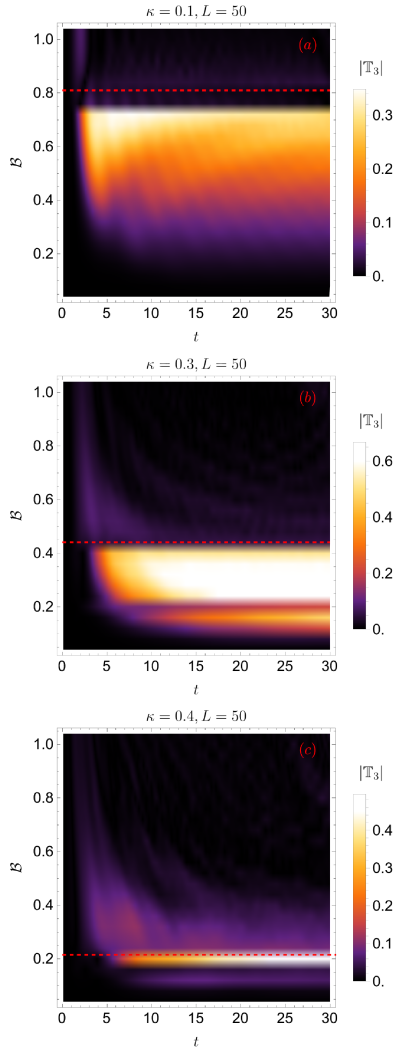


FIG. 9. Variation of Liang formation for the quench starting from the ground state for top- $\kappa = 0.1$ , middle- $\kappa = 0.3$ , bottom- $\kappa = 0.4$ . The rest of the parameters are same as Fig. 4(c)